Engineering Structures 173 (2018) 681–692

Contents lists available at ScienceDirect

Engineering Structures

journal homepage: www.elsevier.com/locate/engstruct

Analytical model for shear strength estimation of reinforced concrete beam-column joints

Leonardo M. Massone*, Gonzalo N. Orrego

Department of Civil Engineering, University of Chile, Blanco Encalada 2002, Santiago, Chile

ARTICLE INFO

Keywords:
Strength
Beam-column
Joint
Shear
Model
Reinforced concrete

ABSTRACT

A model capable of predicting the shear response of beam-column joints subjected to seismic actions is presented. The analytical model, originally developed for walls and based on a simple physical formulation, is adapted. It considers mean stress and strain fields based on a reinforced concrete panel representing the joint, under the assumption that the principal concrete stress and principal strain directions coincide. Simple constitutive material laws are considered for concrete and steel. To estimate the shear capacity, the model satisfies the equilibrium in the longitudinal (vertical) direction. In order to analyze the accuracy of the model, a database integrated by 92 tests of exterior and interior beam-column joints is collected from the literature. Noting that the original model does not consider the effect of confinement product of adjacent elements to the connection, this effect is introduced through factors that reduce the values of the longitudinal and transverse strain used to calibrate the angle of the strut. In addition, the contribution of the transverse reinforcement in the capacity of the element is included. These modifications together with the influence of the boundary reinforcement, yields a good strength estimate for exterior and interior joints that fail in shear. When comparing with other models from the literature, it is observed that the proposed model provides one of the best correlations.

1. Introduction

Beam-column joints are used in frame structures and fulfill the function of delivering continuity to the structure, in addition to transferring shear and moment forces from one structural element to another. For these reasons it is required a correct design of these connections in order to maintain stable structures. Structure collapse can occur when a beam-column joint (reference as joints in the text) fails in shear, which is a brittle failure response (Fig. 1a). Other type of potential failure occurs when one of the elements adjacent to the joint fails before the joint (Fig. 1b).

In frame analysis, most models assume a rigid behavior for beam-column joints, giving only flexibility to column and beam elements. Some previous works have modified the properties of the elements framing into the joint in order to account for the additional joint flexibility (e.g., Hoffmann et al. [1]). Many models have evolved from there incorporating, among others, bond slip observed in the longitudinal reinforcement of beams, confining effect of surrounding elements, and shear response of the joint (e.g., Youssef and Ghobarah [2]); however, for the shear response in some cases only simple models have been included. In order to correctly predict the shear response of the joint, more complete and complex formulations have been included, based on panel response (e.g., modified compression field theory in models such as in Lowes and Altoontash [3] and Pan et al. [4]). Such formulations allow representing the observed failure modes and are intended for nonlinear analysis of elements or entire structures in finite element formulation, rather than shear strength predictions for design.

The current work focuses in the shear strength estimation of beam-column joints for different failure modes. In the literature there are different models to estimate shear response in beam-column joints. Some of them are based on a strut-and-tie model that incorporates forces equilibrium, strain compatibility and the material constitutive laws (e.g., [5,6]). There are also closed-form expressions, some as simple as the one in ACI318-14 [7], semi-empirical expressions such as the model by Kassem [8], and Kim and LaFave [9] that require calibration of parameters and others more elaborated such as the model developed by Wang et al. [10].

Hwang and Lee [5,6] present a strut-and-tie model to predict the shear strength of interior and exterior reinforced concrete joints, which satisfies conditions of equilibrium forces, strain compatibility and constitutive law of cracked concrete. In those works, they propose to model the distribution of stresses of the joint as a statically indeterminate lattice, through three mechanisms: one diagonal, one horizontal and one vertical (Fig. 2). The diagonal mechanism (Fig. 2a)

* Corresponding author.
E-mail address: lmassone@ing.uchile.cl (L.M. Massone).

https://doi.org/10.1016/j.engstruct.2018.07.005
Received 10 March 2017; Received in revised form 9 May 2018; Accepted 2 July 2018
Available online 14 July 2018
0141-0296/ © 2018 Elsevier Ltd. All rights reserved.

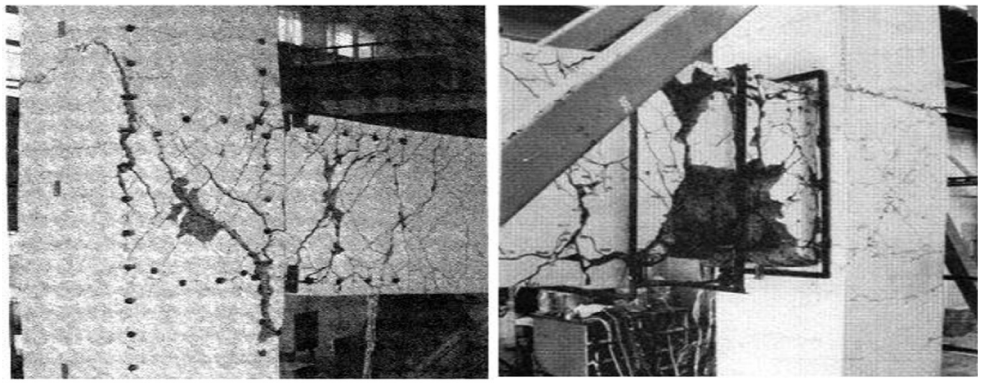

Fig. 1. Type of failure in a joint – (a) Shear failure at the joint [38] and (b) failure of the beam adjacent to the joint in flexure [24].

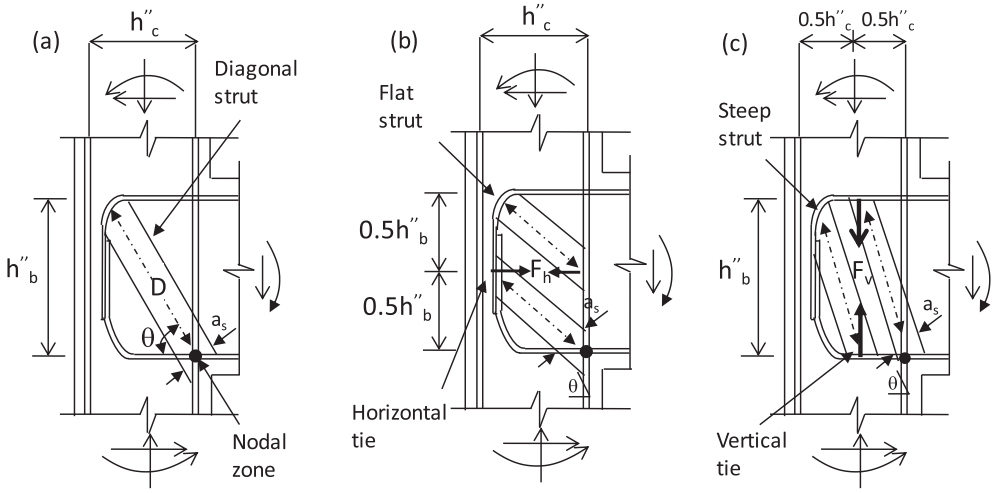

Fig. 2. Shear resistant mechanisms – (a) diagonal mechanism, (b) horizontal mechanism, and (c) vertical mechanism (after [5]).

consists of a diagonal compression strut with an angle of inclination $\theta = \tan^{-1}(h_b''/h_c'')$, where h_b'' and h_c'' (Fig. 2) are the distances between the end longitudinal reinforcements of the beam and the column, respectively. In addition, it is assumed that the direction of the diagonal strut coincides with the main direction of compression of the concrete. The horizontal mechanism (Fig. 2b) consists of a horizontal tie and two flat struts, in which the stirrups of the column constitute the tie. It is also assumed that the stirrups in the core of the joint are considered 100% effective when calculating the area of horizontal reinforcement, while those located at the ends of the joint are considered providing only 50% of their force as effective. The vertical mechanism (Fig. 2c) includes a vertical tie and two steep struts. The vertical tie is considered as the vertical intermediate reinforcement of the column. The combination of the 3 lattices determines the complete system, so that by equilibrium the resulting shear force is defined as,

$$V_{jh} = -D\cos\theta + F_h + F_v\cot\theta \quad (1)$$

where D is the compression force at the diagonal strut; and F_h and F_v are the forces in the horizontal and vertical struts, respectively. As the system is hyperstatic, a load distribution pattern is assumed between the 3 mechanisms.

Failure of the compression strut is defined when the concrete at the end of the diagonal in compression, that is, in the nodal zone (Fig. 2a) reaches its maximum compressive capacity. To determine the capacity, it is necessary to define the constitutive laws of the materials. For concrete, as same as in this work, the ascending branch for the compression curve in the cracked concrete of the model by Zhang and Hsu [11] is considered to characterize the biaxial action present in this material. As for reinforcing steel, its behavior is considered elasto-plastic. When incorporating compatibility, forcing average deformations for the entire element, the nonlinear system requires an iterative process to validate compatibility, which allows determining the shear capacity.

In the ACI 318-14 [7], on the other hand, the shear strength is obtained as a function of the compressive strength of concrete, defined as,

$$V_{jh} = \gamma\sqrt{f_c'}A_j \quad (2)$$

where γ is a function of the confinement delivered by the surroundings beams. For the purpose of this work, where joints with confluent beams on only 1 or 2 sides are considered, for interior joints (beams in 2 faces) $\gamma = 1.2$ if the width of these beams is at least 75% of the width of the joint. In other cases, $\gamma = 1.0$. A_j represents the effective area of the joint, which for beams centered on the joint includes the entire cross-sectional area of the joint.

Another closed-form expression is the model proposed by Wang et al. [10], where it is assumed that the shear capacity of the joint is obtained when the stresses in the concrete, located at point C (Fig. 3) have reached their material failure envelope. The point C is considered only subjected to an axial stress σ_y and a shear stress τ_{xy}. Also, it is assumed that the principal stresses at the joint at the moment of failure, coincide with the two normal stresses acting along and perpendicular to the diagonal strut AB.

On the other hand, the angle α is defined as $\alpha = \tan^{-1}(h_c/h_b)$, where h_c is the width of the column; h_b corresponds to the height of the beam;

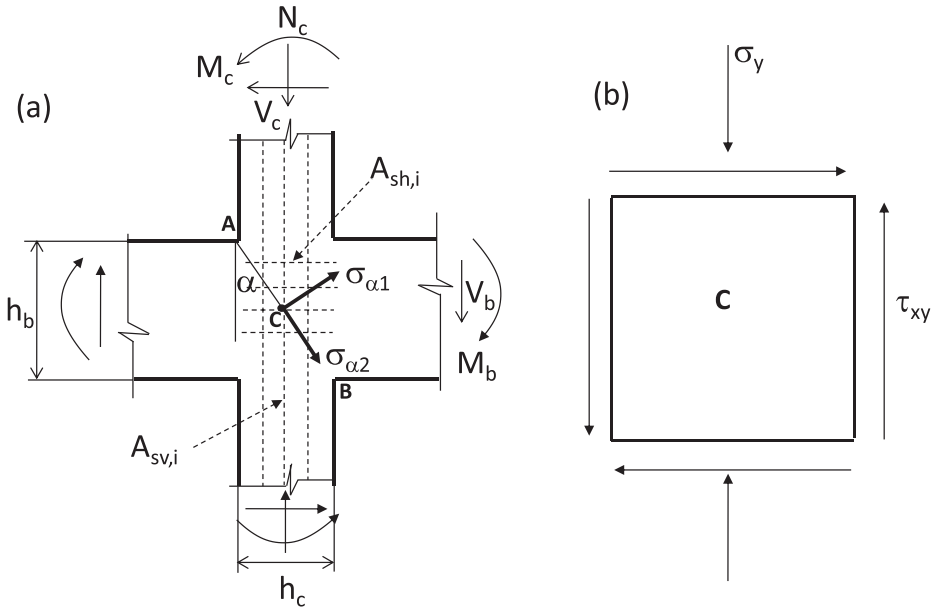

Fig. 3. (a) Forces and mechanism of a beam-column joint; and (b) stress field of point C (after [10]).

$\sigma_y = N_c/b_c h_c$ where N_c is the axial load on the column, b_c is the width of the column; $\tau_{xy} = V_{jh}/b_j h_c$, where V_{jh} is the shear force of the joint in the horizontal direction, b_j is the depth of the joint, considered as the lowest between b_c and $b_b + 0.5h_c$ if $b_c \geq b_b$ or the lowest between b_b and $b_c + 0.5h_c$ if $b_c < b_b$; where b_b is the width of the beam.

In order to incorporate the biaxial behavior of concrete, that is, the effect of tensile stresses on the compressive strength, the Kupfer and Gerstle [12] model is used, which is defined by the failure criterion $\frac{\sigma_{\alpha 1}}{f_{t,n}} - 0.8\frac{\sigma_{\alpha 2}}{f'_c} = 1$, where $\sigma_{\alpha 2}$ is the main compressive stress and $f_{t,n}$ is the nominal tensile stress of concrete in the direction of $\sigma_{\alpha 1}$ (main tensile stress), which considers the contribution of horizontal and vertical distributed reinforcement. Through equilibrium, it defines $f_{t,n} = f_{t,c} + \rho_{sh} f_{yh}\cos^2\alpha + \rho_{sv} f_{yv}\sin^2\alpha$, where ρ_{sh} is the amount of horizontal reinforcement ($A_{sh}/b_j h_b$) that includes the column stirrups between the upper and lower longitudinal reinforcement of the adjacent beam; ρ_{sv} is the amount of vertical reinforcement ($A_{sv}/b_j h_c$) that considers the intermediate longitudinal bars of the column; f_{yh} and f_{yv} are the yield stress of the horizontal and vertical reinforcement, respectively; $f_{t,c} = 0.56\sqrt{f'_c}$, corresponds to the contribution of the concrete to the nominal tensile strength. The model assumes that the tensile strength of concrete is reached and that the horizontal and vertical reinforcements have reached their respective yield stresses.

This gives a closed-form expression for the maximum shear strength of the joint (V_{jh}), as

$$V_{jh} = \beta_j \frac{1.0 - (\sin^2\alpha/f_{t,n} - 0.8\cos^2\alpha/f'_c)\sigma_y}{(1/f_{t,n} + 0.8/f'_c)\sin 2\alpha} b_j h_c \quad (3)$$

In order to take into account the better behavior of the interior joints than the exterior joints (due to the greater confinement effect provided by the adjacent beams in interior joints), a reduction factor (β_j) is introduced in which $\beta_j = 1.0$ for interior joints and 0.8 for exterior joints.

The work by Kassem [8] uses the same principles developed in the strut-and-tie model by Hwang and Lee [5,6], but reduces the expressions to a closed-form solution by imposing the distribution of forces between D, F_h, and F_h as a calibration with test data. Thus, the expression reduces for exterior beam-column joints to,

$$V_{jh} = (0.21\psi\kappa\cos\alpha + 0.09(\omega_h + 3.47\omega_b \frac{b_b}{b_j}\tan\alpha) + 0.22\omega_v \frac{b_b}{b_j}\cot\alpha) f'_c A_j \quad (4)$$

And for interior beam-column joints to,

$$V_{jh} = \left(0.26\psi\kappa\cos\alpha + 0.44\left(\omega_h + 1.39\omega_b \frac{b_b}{b_j}\tan\alpha\right) + 0.07\omega_v \frac{b_b}{b_j}\cot\alpha\right) f'_c A_j \quad (5)$$

where $\psi = 0.6(1 - f'_c\,[\text{MPa}]/250)$ for interior joints and $\psi = 0.48(1 - f'_c\,[\text{MPa}]/250)$ for exterior joints; $\kappa = 0.25 - 0.85 n_c/f'_c$, with n_c the axial stress in the column; $\frac{b_b}{b_j}$ is the beam to joint effective width ratio; $\omega_h = \rho_{jh} f_{yh}/f'_c$, with $\rho_{jh} f_{yh}$ the joint transversal reinforcement strength (steel ratio times the yield stress); $\omega_b = \rho_b f_{yb}/f'_c$, with $\rho_b f_{yb}$ the beam longitudinal reinforcement strength (steel ratio times the yield stress); $\omega_v = \rho_{jv} f_{yv}/f'_c$, with $\rho_{jv} f_{yv}$ the column longitudinal interior reinforcement strength (steel ratio times the yield stress).

The work by Kim and LaFave [9] developed a simple closed-form expression that includes key parameters identified and calibrated with a statistical analysis. The expression, for joints with no eccentricity, reduces to,

$$V_{jh} = 1.31\alpha_t\beta_t(\rho_j f_{yh}/f'_c)^{0.15}(\rho_b f_{yb}/f'_c)^{0.3}(f'_c\,[\text{MPa}])^{0.75} A_j \quad (6)$$

where $\alpha_t = 1.0$ for interior joints and 0.7 for exterior joints; $\beta_t = 1.0$ for cases with none or one transverse beam (out-of-plane) and 1.18 for cases with two transverse beams; $\rho_j f_{yh}$ is the joint volumetric transverse reinforcement strength in the direction of loading (steel ratio times the yield stress).

In this paper, a panel model is validated in the estimation of shear capacity of beam-column joints, which considers the joint as a single element that represents its state with average strain and stress. The model used as a base has its origins in the work carried out by Kassem and Elsheikh [13], originally formulated for short walls and with the main directions (crack or strut direction) calibrated for a database of tests, and which has been generalized to angles of the strut direction based on analysis and measurements of wall deformations in the work of Massone and Ulloa [14], and later modified to incorporate the effect of the main reinforcement (boundary) for corbels [15]. For its application in beam-column joints it is necessary to incorporate the confinement effect provided by the elements adjacent to the joint, in addition to the contribution of the transverse reinforcement that in these cases presents a relevant influence. Thus, the results of the modified model are compared with tests of beam-column joints of a database compiled from the literature, besides of a comparison of the predicted

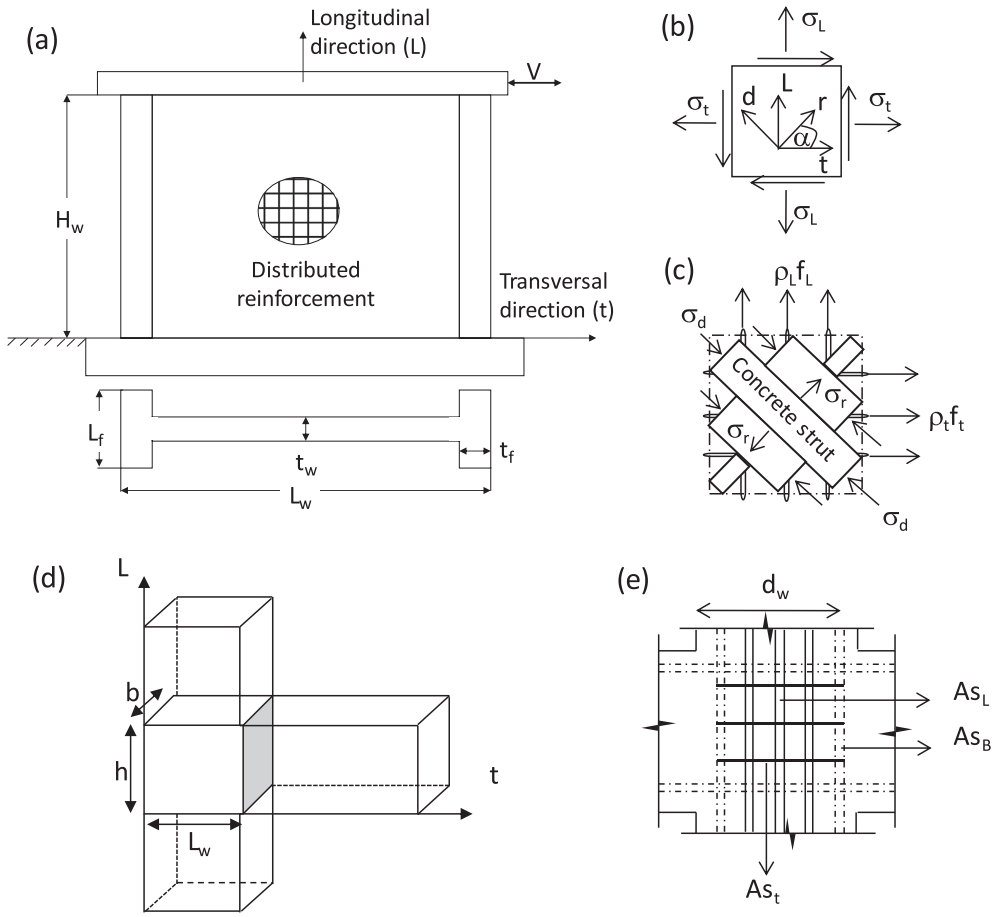

Fig. 4. Wall and beam-column joint analogy – (a) short reinforced concrete wall, (b) average stress on wall, (c) compression strut in wall (after [13]), (d) beam-column joint, and (e) joint reinforcement.

capacity with other available models.

2. Base model and previous modifications

In the model proposed by Kassem and Elsheikh [13], an average strain and stress field is considered for the entire element (wall in this case), applying equations of equilibrium (Fig. 4), strain compatibility and constitutive laws for concrete and reinforcing steel. Using this, the angle of the compression strut, which is assumed equal to the angle of principal stresses and strains, was determined to be the one that best predicts the shear strength for a selected database.

Assuming that the reinforcing steel is only subjected to tensile stresses and that the main stress direction is oriented at an angle α with respect to the vertical direction, the equilibrium equations of the system along the coordinate axis Lt are expressed by (Fig. 4b and c):

$$\sigma_L = \sigma_d \cos^2\alpha + \sigma_r \sin^2\alpha + \rho_L f_L \tag{7}$$

$$\sigma_t = \sigma_d \sin^2\alpha + \sigma_r \cos^2\alpha + \rho_t f_t \tag{8}$$

$$\tau_{Lt} = (-\sigma_d + \sigma_r)\cos\alpha\sin\alpha \tag{9}$$

where σ_L, σ_t are the normal stresses in the directions L and t [MPa]; τ_{Lt} corresponds to the average shear stress in the L-t plane [MPa]; σ_d, σ_r are the principal concrete stresses in the directions d and r [MPa]; f_L, f_t correspond to the average stresses of the reinforcing steel in the directions L and t [MPa]; and ρ_L, ρ_t are the steel ratio in the L and t directions.

Considering that the stress distribution in the joint is uniform, the shear force is obtained as:

$$V = \tau_{Lt} t_w d_w \tag{10}$$

where V corresponds to the shear force in the section [N]; t_w is the thickness of the element [mm]; d_w is the horizontal length of the wall between the centroids of the boundary elements [mm], or d_w can be calculated as 0.8 L_w, where L_w is the length of the wall.

For the strain field, where perfect bond between concrete and steel is assumed, the expressions are defined as:

$$\varepsilon_L = \varepsilon_d \cos^2\alpha + \varepsilon_r \sin^2\alpha \tag{11}$$

$$\varepsilon_t = \varepsilon_d \sin^2\alpha + \varepsilon_r \cos^2\alpha \tag{12}$$

$$\gamma_{Lt} = 2(-\varepsilon_d + \varepsilon_r)\cos\alpha\sin\alpha \tag{13}$$

where ε_L, ε_t are the strain in the L and t directions; γ_{Lt} corresponds to the shear strain in the L-t plane; ε_d, ε_r are the principal strain in the d and r directions (positive for tensile strain).

Finally, assuming that the top displacement of the wall (Δ [mm]) is controlled by shear, its value is determined as:

$$\Delta = \gamma_{Lt} H_w \tag{14}$$

where H_w corresponds to the height of the wall [mm].

In order to determine the concrete stress in compression, the constitutive law by Zhang and Hsu [11] is considered, which considers the strength degradation of concrete due to tensile strain in the orthogonal direction (ε_r). Thus, the equations representing this behavior are as follows:

$$\sigma_d = -\zeta f_c' \left[2\left(\frac{-\varepsilon_d}{\zeta\varepsilon_o}\right) - \left(\frac{-\varepsilon_d}{\zeta\varepsilon_o}\right)^2 \right] \quad \text{If} \quad \varepsilon_o \leqslant \zeta\varepsilon_o \tag{15}$$

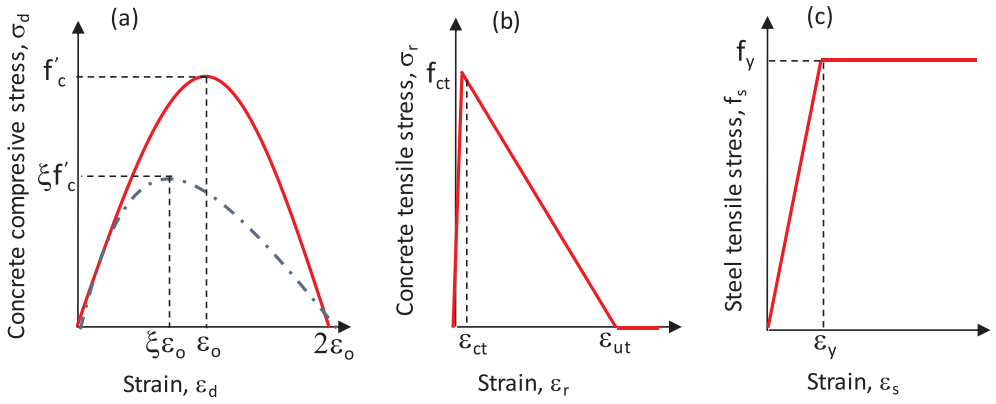

Fig. 5. Material laws – (a) concrete in compression [11]; (b) concrete in tension [16], and (c) reinforcing steel.

$$\sigma_d = -\zeta f_c' \left[1 - \left(\frac{\frac{-\varepsilon_d}{\zeta\varepsilon_o} - 1}{\frac{2}{\zeta} - 1}\right)^2\right] \quad \text{If} \quad \zeta\varepsilon_o < \varepsilon_o \leqslant 2\zeta\varepsilon_o \tag{16}$$

where $\zeta = \frac{5,8}{\sqrt{f_c'}} \frac{1}{\sqrt{1+400\varepsilon_r}} \leqslant \frac{0,9}{\sqrt{1+400\varepsilon_r}}$ is the reduction coefficient; f_c' corresponds to the maximum compression stress of a standard concrete cylinder [MPa]; $\varepsilon_o = 0.002$ corresponds to the strain associated with f_c'.

As for the constitutive law for concrete in tension, the proposal by Gupta and Rangan [16] is adopted:

$$\sigma_r = E_c \varepsilon_r \quad \text{If} \quad 0 \leqslant \varepsilon_r \leqslant \varepsilon_{ct} \tag{17}$$

$$\sigma_r = f_{ct}' \left(\frac{\varepsilon_{ut} - \varepsilon_r}{\varepsilon_{ut} - \varepsilon_{ct}}\right) \quad \text{If} \quad \varepsilon_{ct} \leqslant \varepsilon_r \leqslant \varepsilon_{ut} \tag{18}$$

where $f_{ct}' = 0.4\sqrt{f_c' \text{ [MPa]}}$ is the maximum tensile stress in concrete [MPa]; $E_c = 4700\sqrt{f_c' \text{ [MPa]}}$ corresponds to the concrete modulus of elasticity [MPa]; $\varepsilon_{ct} = f_{ct}'/E_c$ is the cracking strain; $\varepsilon_{ut} = 0.002$ corresponds to the ultimate concrete strain. In Fig. 5(a) and (b) the stress-strain curves corresponding to the concrete behavior in compression and tension, respectively, are shown.

The constitutive law of the reinforcing steel is modeled as perfect elasto-plastic (Fig. 5c). Thus, the equations that describe this model are:

$$f_s = E_s \varepsilon_s \quad \text{If} \quad \varepsilon_s < \varepsilon_y \tag{19}$$

$$f_s = f_y \quad \text{If} \quad \varepsilon_s \geqslant \varepsilon_y \tag{20}$$

where f_s is the steel stress [MPa]; $E_s = 200$ [GPa] corresponds to the elastic modulus of steel; ε_s is the strain of the steel; f_y is the yield stress of steel [MPa].

Given the strut angle, for each value of the shear strain γ_{Lt}, the strain of the strut ε_d is varied until the vertical equilibrium equation is satisfied ($\sigma_L = \frac{N}{A}$, where N is the applied vertical load and A is the cross-sectional area of the wall). In this way the model allows to obtain the complete load-displacement curve, since for each deformation state the tension state of the reinforced concrete panel is known.

Massone and Ulloa [14] proposed a new way of obtaining the crack or strut angle, based on strain estimates from analysis that have been validated experimentally for walls. On the other hand, Massone and Álvarez [15] used the modified panel model for reinforced concrete walls with corbel. For this, the model was adapted and modified in order to obtain better results, in terms of a good prediction of capacity and a low standard deviation. The angle of the strut in this case was modified to correctly capture its value for geometric parameters and reinforcing amounts that were different from those observed in the case of walls. For walls clamped at both ends, the horizontal and vertical average strain are defined by [17],

$$\varepsilon_t = 0.0023(100\rho_t + 0.25)^{-0.53}\left(\frac{H_w}{L_w} + 0.5\right)^{0.47}\left(\frac{100N}{f_c' t_w L_w} + 5\right)^{0.25}(100\delta)^{1.4} \tag{21}$$

$$\varepsilon_L = 0.0094(100\rho_t + 0.25)^{-0.17}\left(\frac{H_w}{L_w} + 0.5\right)^{-0.16}\left(\frac{100N}{f_c' t_w L_w} + 5\right)^{-0.35}(100\delta) + eN \tag{22}$$

where ρ_t is the transverse steel ratio; $\delta = \Delta/H_w$is the lateral drift (assumed as pure shear distortion, $= \gamma_{Lt}$), and eN the elastic vertical deformation due to the axial load.

Another important modification corresponds to the incorporation of the boundary reinforcement in the analysis, since in the work by Massone and Ulloa [14] it was reported that there was an underestimation of the shear strength as the strength associated with the boundary element increased.

One way of incorporating the effect of the main or boundary reinforcement is to rewrite the equation of longitudinal equilibrium (Eq. (4)) as follows:

$$\sigma_L = \sigma_d \cos^2\alpha + \sigma_r \sin^2\alpha + \rho_L f_L + \beta\rho_B f_B \tag{23}$$

where f_B is the stress of the main or boundary reinforcement in the direction L [MPa] (associated to the same web longitudinal strain, ε_L); ρ_B is the main or boundary reinforcement ratio; β is the main reinforcement efficiency parameter ($0 \leq \beta \leq 1$). Massone and Álvarez [15], based on a good estimate of the shear capacity for corbels, concluded that β should take the value of 0.3.

3. Modified panel model for beam-column joints

At first, it is necessary to make a geometric analogy between a short wall and a beam-column joint. As shown in Fig. 4(d), the cubic element represents the joint, such that the following similarities can be made: h = H_w and b = t_w. In addition, in Fig. 4(e), the reinforcement bars in the joint are illustrated. Three types of reinforcement are distinguished: the transverse reinforcement (As_t), the longitudinal reinforcement (As_L) and the edge reinforcement (As_B).

3.1. Modification of the tensile constitutive law of concrete

A preliminary analysis of the results indicates that the model with the modifications incorporated has good results, however, the impact of the horizontal reinforcement is not captured adequately (the amount of reinforcement reaches values of 3% in the database in some cases, which was not observed in walls). This occurs because the equilibrium is realized in the vertical direction, and indirectly and partially, the effect is captured in the estimate of the horizontal strain (expansion) that is used to determine the angle of the compression strut. To directly

Table 1
Exterior and interior joint test comparison.

Type	h (mm)	L_w (mm)	b (mm)	b_b (mm)	f'_c (MPa)	ρ_L (%)	f_{yL} (MPa)	ρ_t (%)	f_{yt} (MPa)	ρ_B (%)	f_{yB} (MPa)	$N/A_g f'_c$	V_{test} (kN)
Exterior	480	300	300	259	33.6	0.78	490	0.87	437	1.17	490	0.06	554
Interior	419	362	362	279	34.3	0.87	414	0.76	352	1.29	414	0.05	840

incorporate this effect into the analysis, the expression by Wang et al. [10] to define the tensile capacity of concrete is used. This expression, through equilibrium, incorporates both the contribution of vertical and horizontal distributed reinforcement. For the purposes of this analysis, and considering that vertical reinforcement is already incorporated in the equilibrium equation, only the horizontal reinforcement component is incorporated in this term. In this way, the tensile strength of concrete is defined as:

$$f_{t,n} = 0.4\sqrt{f'_c\ [\text{MPa}]} + \rho_{sh} f_{yh} \cos^2 \alpha \tag{24}$$

3.2. Effect of confinement of beams and columns adjacent to the joint

As reported in the literature (e.g. [10,18]) the interior joints present higher shear capacity than the external joints under similar conditions, because of their higher confining effect (constraining expansion) of adjacent beams. This can be seen with the 1B (exterior – [19]) and X1 (interior – [20]) tests, where the interior and exterior joints are designed similarly. Table 1, which shows the most relevant parameters of the tests, indicates that the interior joint reaches a shear strength 52% higher than the exterior joint. The proposed model, after incorporating the confinement effect, provides similar joint shear strength estimates (807 kN for the interior joint vs. 499 kN for the exterior joint), mainly attributed to confinement.

Additionally, in the present work, it is considered that the columns, as same as the beams, can provide some vertical (longitudinal) confinement to the joint. In this case, both exterior and interior joints have the same elements above and/or below the joint, so this effect must influence in a similar way both types of connections. Thus, in order to incorporate the confinement influence provided by the beams and columns, Eqs. (21) and (22) were modified, such that $\varepsilon^{mod}_{t,avg} = \varepsilon_{t,avg}(1-\lambda_t)$ and $\varepsilon^{mod}_{L,avg} = \varepsilon_{L,avg}(1-\lambda_L)$, reducing their values, which is understood as a limitation in the transverse and longitudinal expansion of the joint by means of factors λ_t (for the transverse direction) and λ_L (for the longitudinal), which vary from the value 0 to 1.

These equations are used to obtain and calibrate the angle of the strut (crack angle), α. It is assumed that the compression strut angle is defined when $\sigma_r = f_{ct}$ is reached, as same as with previous models. Therefore, in this model, the confinement from beams and columns is reflected in the expressions that calculate this angle. In order to set the parameter values of λ_t and λ_L, a database of interior and exterior beam-column joint tests was compiled (this is described in the following section). While applying the modified model the pair of values that best estimates the shear strength of joint with low scatter was selected. Considering that both exterior and interior joints have the same confinement due to the presence of columns (not beams), the value of the constant reducing the longitudinal expansion, $\lambda_L = 0.5$ is selected for both types of joint. On the other hand, as for the exterior joints ($\lambda_t = 0.2$) there are fewer beam elements in the transverse direction than those in interior joint, there is a higher level of confinement for interior joint ($\lambda_t = 0.7$), resulting in a higher value of λ_t.

These parameters allow determining the new values of vertical and horizontal average strain for beam-column joints. As it was done by a previous author [14], given a guess value for the shear distortion (γ_{Lt}), the longitudinal and transverse strain can be determined with the modified expressions of Eqs. (21) and (22), for a specific element configuration (different values of geometries, axial load, material properties and reinforcement amounts). By using compatibility and the material constitutive law for concrete in tension, it can be determine whether the cracking stress has been reached ($\sigma_r = f_{ct}$), increasing the value of γ_{Lt} until the crack has formed, which defines the crack angle (α). After running this procedure, the new expressions for the cracking angles (strut) are calibrated as a function of the most relevant parameters (aspect ratio and axial load level), as:

Exterior joint:

$$\alpha = 17.6\left(\frac{h}{L_w} + 0.5\right)^{-0.02}\left(\frac{N}{f'_c bL_w} + 0.1\right)^{-0.46} \tag{25}$$

Interior joint:

$$\alpha = 19.8\left(\frac{h}{L_w} + 0.5\right)^{-0.04}\left(\frac{N}{f'_c bL_w} + 0.1\right)^{-0.43} \tag{26}$$

3.3. Description of the database

A large series of research projects available from the literature are used to compile a database for interior and exterior beam-column joints [18–39]. The compiled database consists of 92 tests, with 54 exterior joints and 38 interior joints (Table 2). The two types of joints and testing scheme are shown in Fig. 6. For the database, the compressive strength of concrete varies from 22.1 to 92.4 [MPa]; the longitudinal reinforcing steel ratio varies from 0 to 4%; the boundary steel reinforcement ratio varies from 0.51 to 3.5%; the transverse reinforcement steel ratio varies from 0 to 3%; the yield stress of the longitudinal and boundary reinforcement steel varies from 280 to 644 [MPa]; whereas for the transverse reinforcing steel it varies from 235 to 1320 [MPa]; the axial load level varies from 0 to $0.75L_w b f'_c$. The database is compiled from several research programs, with a variety of steel quantities (low to high steel ratio), material strength (normal to high strength materials), as well as axial load, which makes the database rich in data that can identify the relevance of each parameter in the model.

3.4. Flexure model for beams and flexo-compression model for columns

In order to verify whether the beams or columns adjacent to the joint fail before the joint, a simple bending model is implemented in the case of the beams and one of flexo-compression for the columns. In both cases, it is considered that failure occurs at the joint-beam or joint-column interface, respectively. The procedure described in the ACI 318-14 [7] is used in the analysis. Once the ultimate strength is obtained, either from the beam or column, the forces acting on the joint are represented by Fig. 7, such that the joint shear strength is determined as $V_{joint} = T_{s,b2} - V_{c1}$, for exterior joints and $V_{joint} = T_{s,b1} + T_{s,b2} - V_{c1}$ for interior joint, where V_{c1} represents the shear force in the column, and $T_{s,b1}$ and $T_{s,b2}$ correspond to the tensile forces of the upper and lower beam reinforcement, respectively.

4. Modified model results

4.1. Strength

Using the proposed model and incorporating the contribution of the boundary reinforcement proposed by Massone and Alvarez [15], that is, taking β = 0.3, as well as, incorporating the horizontal reinforcement in the tensile strength of concrete and implementing the new expressions to obtain the crack angle (strut) (Eqs. (25) and (26)), the shear

Table 2
Beam-column joint database.

Author	Specimen	ID	h [mm]	L_w [mm]	b [mm]	d_w [mm]	b_{viga} [mm]	f'_c [MPa]	ρ_L [%]	f_{yL} [MPa]	ρ_t [%]	f_{yt} [MPa]	ρ_B [%]	f_{yB} [MPa]	$N/(A_g f'_c)$	V_{test} [kN]	Type[a]
Magget [22]	Unit A	1	460	380	330	290	255	22.1	0.81	365	1.61	317	1.22	365	0.07	576	1
Lee et al. [19]	2	2	254	279	203	229	203	29.0	0.00	0	1.11	389	1.23	538	0.11	194	1
	5	3	254	279	203	229	203	24.8	0.00	0	1.11	389	1.23	538	0.00	206	1
	6	4	254	279	203	229	203	24.8	0.00	0	0.49	273	1.23	531	0.00	208	1
Paulay et al. [29]	Unit 1	5	610	457	457	412	356	22.6	0.67	296	0.90	326	0.67	296	0.05	754	1
	Unit 2	6	610	457	457	412	356	22.5	0.67	296	0.90	326	0.67	296	0.15	990	1
	Unit 3	7	610	457	457	412	356	26.9	0.67	296	0.46	316	0.67	296	0.05	753	1
Park et al. [28]	Unit 3	8	457	406	305	368	229	38.2	0.56	485	0.22	321	0.36	315	0.10	606	1
Kanada et al. [16]	U40L	9	380	300	300	259	260	24.3	1.00	385	0.00	0	1.00	385	0.00	256	1
	U41L	10	380	300	300	259	260	26.7	1.00	385	0.26	294	1.00	385	0.00	339	1
	U42L	11	380	300	300	261	260	30.1	0.99	385	0.13	294	0.99	385	0.00	337	1
	U20L	12	380	300	300	261	260	26.7	0.00	0	0.00	0	0.73	387	0.00	188	1
	U21L	13	380	300	300	261	260	30.1	0.00	0	0.26	294	0.73	387	0.00	198	1
Ehsani et al. [9]	1B	14	480	300	300	244	259	33.6	0.78	490	0.87	437	1.17	490	0.06	554	1
	3B	15	480	300	300	244	259	40.9	0.78	490	1.31	437	1.17	490	0.06	591	1
	4B	16	439	300	300	244	259	44.6	0.78	490	1.48	437	1.56	490	0.06	635	1
	5B	17	480	340	340	290	300	24.3	1.03	414	0.77	437	2.06	414	0.13	571	1
	6B	18	480	340	340	290	300	39.8	0.58	490	0.77	437	0.87	490	0.07	469	1
Zerbe [35]	J1	19	381	305	305	241	254	39.4	1.38	483	1.09	531	2.07	483	0.05	438	1
	J3	20	381	305	305	241	254	39.9	1.38	483	1.09	531	2.07	483	0.05	449	1
Ehsani et al. [10]	1	21	480	340	340	290	300	64.7	0.58	455	1.15	455	1.08	455	0.02	486	1
	2	22	480	340	340	290	300	67.3	0.58	455	1.15	455	1.08	455	0.04	609	1
	3	23	439	300	300	249	259	64.7	0.76	455	1.48	455	1.42	455	0.07	542	1
	4	24	439	300	300	249	259	67.3	1.04	455	1.48	455	1.88	455	0.05	627	1
Alameddine [3]	LL8	25	508	356	356	292	317	56.5	0.75	479	1.20	446	1.35	468	0.04	860	1
	LH8	26	508	356	356	292	317	56.5	0.75	479	1.80	446	1.35	468	0.04	838	1
	HL8	27	508	356	356	292	317	56.5	0.98	457	1.22	446	1.46	457	0.07	987	1
	HH8	28	508	356	356	292	317	56.5	0.98	457	1.84	446	1.46	457	0.07	986	1
	LL11	29	508	356	356	292	317	74.5	0.75	479	1.14	446	1.35	468	0.03	769	1
	LH11	30	508	356	356	289	317	74.5	0.76	479	1.77	446	1.36	468	0.03	934	1
	HL11	31	508	356	356	289	317	74.5	0.99	457	1.16	446	1.48	457	0.06	967	1
	HH11	32	508	356	356	289	317	74.5	0.99	457	1.77	446	1.48	457	0.06	1021	1
Alameddine [3]	LL14	33	508	356	356	286	317	92.4	0.76	479	1.22	446	1.38	468	0.02	878	1
	LH14	34	508	356	356	292	317	92.4	0.75	479	1.80	446	1.35	468	0.02	890	1
	HH14	35	508	356	356	292	317	92.4	0.98	457	1.87	446	1.46	457	0.04	1032	1
Fujii et al. [12]	B1	36	250	220	220	190	160	30.0	1.22	387	0.41	291	1.22	387	0.07	246	1
	B2	37	250	220	220	190	160	30.0	1.22	387	0.41	291	1.22	387	0.07	214	1
	B3	38	250	220	220	190	160	30.0	1.22	387	0.41	291	1.22	387	0.24	273	1
	B4	39	250	220	220	190	160	30.0	1.22	387	1.10	291	1.22	387	0.24	287	1
Kaku et al. [15]	1	40	220	220	220	201	160	31.1	0.00	0	0.49	250	0.90	360	0.17	249	1
	2	41	220	220	220	201	160	41.7	0.00	0	0.49	250	0.90	360	0.10	244	1
	3	42	220	220	220	201	160	41.7	0.00	0	0.49	250	0.90	360	0.00	212	1
	4	43	220	220	220	201	160	44.7	0.00	0	0.12	281	0.90	360	0.17	236	1
	5	44	220	220	220	201	160	36.7	0.00	0	0.12	281	0.90	360	0.09	220	1
	6	45	220	220	220	201	160	40.4	0.00	0	0.12	281	0.90	360	0.00	208	1
	7	46	220	220	220	204	160	32.2	0.70	395	0.49	250	0.70	395	0.12	249	1
	8	47	220	220	220	204	160	41.2	0.70	395	0.49	250	0.70	395	0.08	243	1
	9	48	220	220	220	204	160	40.6	0.70	395	0.49	250	0.70	395	0.00	234	1

(*continued on next page*)

Table 2 (*continued*)

Author	Specimen	ID	h [mm]	L_w [mm]	b [mm]	d_w [mm]	b_{viga} [mm]	f'_c [MPa]	ρ_L [%]	f_{yL} [MPa]	ρ_t [%]	f_{yt} [MPa]	ρ_B [%]	f_{yB} [MPa]	$N/(A_g f'_c)$	V_{test} [kN]	Type[a]
	10	49	220	220	220	204	160	44.4	0.70	395	0.12	281	0.70	395	0.17	241	1
	11	50	220	220	220	204	160	41.9	0.70	395	0.12	281	0.70	395	0.08	229	1
	12	51	220	220	220	204	160	35.1	0.70	395	0.12	281	0.70	395	0.00	207	1
	14	52	220	220	220	204	160	41.0	0.28	381	0.12	281	0.28	282	0.08	224	1
	15	53	220	220	220	204	160	39.7	0.32	381	0.12	281	0.32	395	0.08	229	1
	16	54	220	220	220	204	160	37.4	1.13	381	0.49	250	1.13	381	0.00	250	1
Blakeley et al. [6]	interior	55	889	686	457	606	457	48.5	2.36	289	1.52	297	1.77	289	0.03	1722	2
Meinheit et al. [23]	I	56	457	457	330	384	279	26.2	1.22	457	0.50	409	0.61	457	0.40	1090	2
	II	57	457	457	330	374	279	41.8	2.65	449	0.50	409	1.33	449	0.25	1597	2
	III	58	457	457	330	371	279	26.6	4.94	402	0.50	409	1.65	402	0.39	1228	2
	IV	59	457	330	457	251	406	36.1	1.12	438	0.73	409	2.25	438	0.30	1454	2
	V	60	457	457	330	374	279	35.9	2.65	449	0.50	409	1.33	449	0.04	1530	2
	VI	61	457	457	330	374	279	36.8	2.65	449	0.50	409	1.33	449	0.48	1646	2
	VII	62	457	330	457	251	406	37.2	1.12	438	0.73	409	2.25	438	0.47	1468	2
	XII	63	457	457	330	374	279	35.2	2.65	449	2.36	423	1.33	449	0.30	1948	2
	XIII	64	457	457	330	374	279	41.3	2.65	449	1.51	409	1.33	449	0.25	1557	2
Meinheit et al. [23]	XIV	65	457	330	457	251	406	33.2	1.12	438	2.18	409	2.25	438	0.32	1539	2
Fenwick [11]	Unit 1	66	300	300	250	260	200	42.9	0.62	318	2.55	275	1.93	280	0.00	521	2
	Unit 3	67	300	300	250	264	200	39.3	1.37	318	3.00	275	0.69	318	0.00	437	2
Birss [7]	B1	68	610	457	457	–	356	27.9	0.96	427	1.21	346	0.96	427	0.05	1217	2
	B2	69	610	457	457	–	356	31.5	0.96	427	0.50	398	0.96	427	0.44	1213	2
Beckingsale [5]	B11	70	610	457	457	414	356	35.9	0.82	423	2.85	336	0.82	423	0.04	965	2
	B12	71	610	457	457	414	356	34.6	0.82	422	2.85	336	0.82	422	0.04	982	2
	B13	72	610	457	457	414	356	31.4	0.82	398	1.91	336	0.82	398	0.26	1015	2
Park et al. [27]	interior	73	457	406	305	366	229	34.0	0.56	412	2.13	305	0.56	412	0.24	966	2
Park et al. [28]	Unit 1	74	457	406	305	364	229	41.3	0.82	473	3.52	320	0.82	473	0.10	1001	2
Durrani et al. [8]	X1	75	419	362	362	–	279	34.3	0.87	414	0.76	352	1.29	414	0.05	840	2
	X2	76	419	362	362	–	279	33.6	0.87	414	1.15	352	1.29	414	0.06	853	2
	X3	77	419	362	362	–	279	31.0	0.48	345	0.76	352	0.90	345	0.05	629	2
Otani et al. [25]	C1	78	300	300	300	264	200	25.6	1.28	422	0.27	324	0.64	422	0.08	436	2
	C2	79	300	300	300	264	200	25.6	1.28	422	0.90	324	0.64	422	0.08	432	2
	C3	80	300	300	300	264	200	25.6	1.28	422	2.01	324	0.64	422	0.08	410	2
Abrams [1]	LIJ3	81	343	457	343	402	343	31.1	0.00	470	0.55	400	0.57	470	0.00	724	2
	LIJ4	82	343	457	343	402	343	34.3	0.00	470	0.55	400	0.57	470	0.00	789	2
Leon [20]	BCJ2	83	305	254	254	–	203	30.3	1.31	448	0.49	414	0.87	448	0.00	358	2
	BCJ3	84	305	305	254	–	203	27.4	1.09	448	0.49	414	0.73	448	0.00	394	2
	BCJ4	85	305	356	254	–	203	27.2	0.62	448	0.49	414	0.62	448	0.00	462	2
Kitamaya et al. [18]	B1	86	300	300	300	–	200	24.5	1.47	351	0.35	235	1.24	351	0.08	570	2
	B2	87	300	300	300	–	200	24.5	1.47	351	0.35	235	1.24	351	0.08	570	2
	B3	88	300	300	300	–	200	24.5	0.94	371	0.88	235	0.78	371	0.08	515	2
Fujii et al. [12]	A1	89	250	220	220	190	160	40.2	1.82	644	0.41	291	1.52	644	0.08	412	2
	A2	90	250	220	220	190	160	40.2	1.82	387	0.41	291	1.52	387	0.08	380	2
	A3	91	250	220	220	190	160	40.2	1.82	644	0.41	291	1.52	644	0.23	412	2
	A4	92	250	220	220	190	160	40.2	1.82	644	1.10	291	1.52	644	0.23	421	2

[a] Type 1 = Exterior joint/Type 2 = Interior joint.

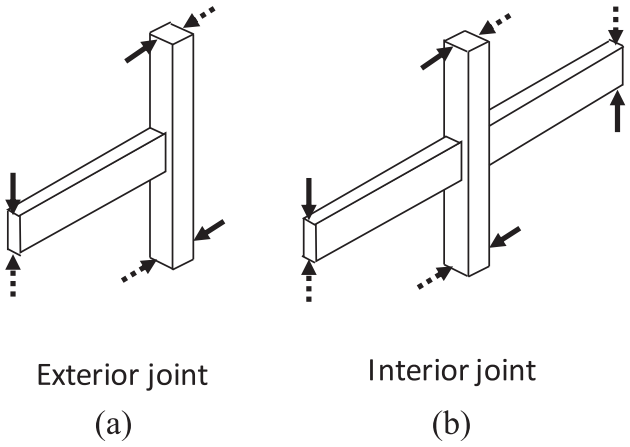

Fig. 6. Types of beam-column joints – (a) exterior joint, and (b) interior joint (after [23]).

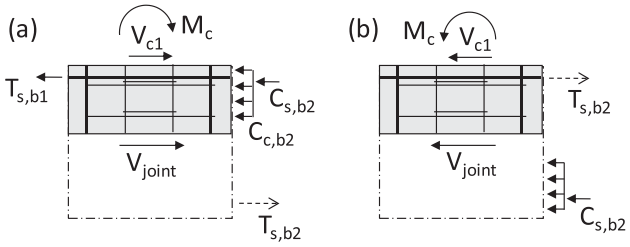

Fig. 7. Forces acting at the joint – (a) interior joint, and (b) exterior joint.

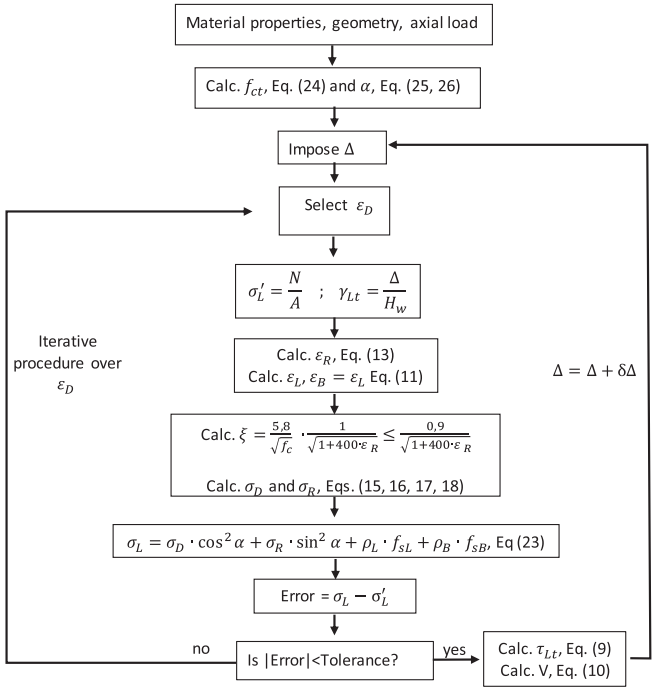

Fig. 8. Flow chart with the numerical scheme of the model formulation.

strength is calculated for the collected database, as well as the strength for the flexural and flexo-compression models. The numerical procedure is described in Fig. 8, where the general steps are described. In order to iterate to solve the vertical equilibrium equation, any numerical (e.g., Newton-Rapson, bisection) can be implemented. Once the overall shear stress versus shear strain is determined, the shear strength is selected as the peak capacity. The response of 3 selected specimens with different failure modes are depicted in Fig. 9. In the figure, one of

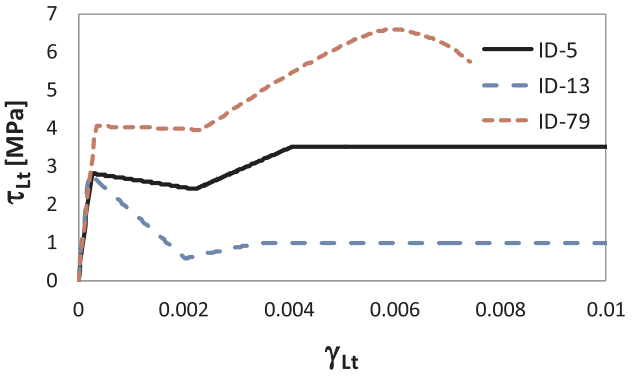

Fig. 9. Analytical shear stress versus shear strain response of selected specimens.

the specimens reaches the tensile capacity of concrete followed by a strength reduction due to the absence of longitudinal distributed reinforcement (ID-13); another specimen also presents strength reduction once tensile of concrete is reached, but recovers its capacity reaching a larger strength due to yielding of the longitudinal reinforcement (ID-5); and similarly, the third specimens overcomes the cracking capacity, but the longitudinal reinforcement due to its larger quantity, does not yield resulting in a joint that reaches the compressive strength of concrete (ID-79).

Table 3 shows the summary of the statistical results (mean and standard deviation of the V_{model}/V_{test} ratio) when applying the model. When comparing the three types of failure modes (joint shear, beam flexure or column flexo-compression), it is observed that for the database there are no predicted tests that have a column failure (not shown in table).

Considering all cases (joint shear and beam flexural failure) yield on average that the capacity predictions for the database are underestimated by 3%. Now, if only joint shear failure is considered, a more conservative prediction is observed, since it underestimates the joint shear strength by 7%. As for beam flexural failure, the model agrees well with the test results (error of 2%), although with greater dispersion than in the case of shear (0.19 versus 0.14), with almost half of the database failing in joint shear. On the other hand, similar accuracy is shown between interior and exterior joints, with more conservative results for interior joints failing in shear.

4.2. Confinement effect from beams

General trends of the two models implemented is provided, that is, the original model where the angle of the strut is not affected by the confinement generated by the adjacent beams (original model) and the model presented in this work that corrects the angle with respect to the level of confinement provided by the beams (both considering the contribution of the boundary and transverse reinforcement), given by the ratio $conf = \frac{b_v}{b_c} \cdot \frac{N}{4}$, where b_v corresponds to the width of the beam, b_c

Table 3
V_{model}/V_{test} ratio results for exterior and interior joints.

	All		Joint shear			Beam flexure		
Type	Avg	Std. Dev.	Avg	Std. Dev.	N° cases (%)	Avg	Std. Dev.	N° cases (%)
Exterior	0.99	0.18	0.98	0.13	23 (43%)	1.00	0.22	31 (57%)
Interior	0.95	0.15	0.89	0.13	24 (63%)	1.05	0.13	14 (37%)
All	0.97	0.17	0.93	0.14	47 (51%)	1.02	0.19	45 (49%)

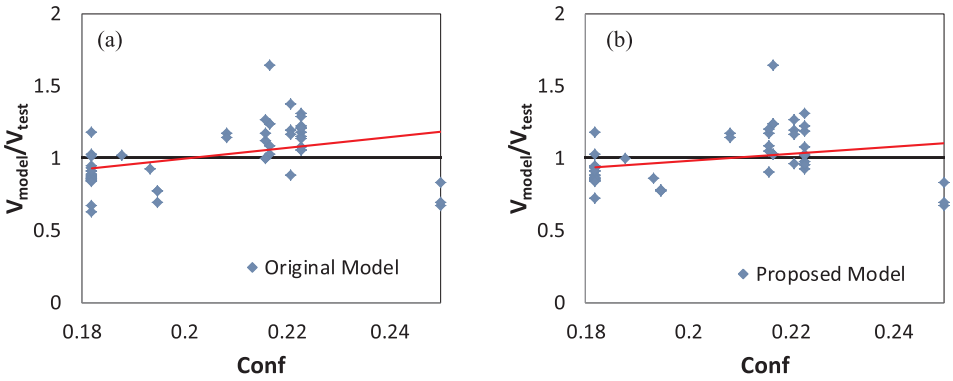

Fig. 10. V_{model}/V_{test} ratio respect to confinement level for exterior joints – (a) original model, and (b) modified model.

to the width of the column and N to the number of beams surrounding the joint.

For a better analysis of this parameter, interior and exterior joints are presented independently. Fig. 10 shows the strength predictions for different confinement levels provided by the beams in exterior joints. This type of exterior joints is not considered confined by the beams in ACI 318-14 [7]. This is mainly reflected in the model, where a trend line (red line) is almost horizontal for both the original and the modified model, with a slight correction in the modified model. This indicates a low dependency on this parameter. On the other hand, Fig. 11 shows the strength predictions for interior joints. ACI 318-14 in this case improves the joint strength due to confinement. This time, the original model is highly dependent on this parameter, observing that as there is more confinement, the model becomes more conservative. This indicates that the original model fails to correctly capture the confinement effect provided by beams. This is corrected when using the modified model, resulting in a trend line (red line) more horizontal than in the case of the original model.

4.3. Comparison with models from the literature

The experimental joint shear strength of the database is compared with five models from the literature, for both exterior and interior joints. These models are: ACI318-14 [7], the work done by Hwang and Lee [5,6], the one by Kassem [8], the model developed by Kim and LaFave [9] and the model presented by Wang et al. [10], which were presented in the introduction. The model results are plotted in Fig. 12. In addition, in all cases, predictions for flexural failure in beams and flexo-compression in columns are also performed. The figure shows that the proposed model and the models by Wang et al. [10], Kassem [8] and Kim and LaFave [9] present average strength ratio close to 1 for joint shear failure (red dots).

Table 4 classifies the strength estimated by failure type for all four models. It is observed that flexo-compression failure in columns is practically inexistent, except for the model by Hwang and Lee [5,6], Kassem [8] and Wang et al. [10], presenting 1 case in each of them. Most cases are controlled by joint shear failure, except for the model by Kim and LaFave [9]. In addition, statistical results (mean and standard deviation) of the model to test strength ratio (V_{model}/V_{test}) for the six models are presented. This ratio was selected, since it is strength independent (instead of comparing V_{model} vs V_{test}). It is observed that the model developed in ACI318-14 presents lowest strength ratio, underestimating the capacity by 17% for all specimens, with the highest dispersion in the group. On the other hand, the proposed model and the model by Wang et al. [10], as well as the semi-empirical models (Kassem [8] and Kim and LaFave [9]) show the best strength ratio (error on average less than 10%) for shear failure with also low standard deviation (between 0.13 and 0.15), with slightly better response in the model by Kim and LaFave, in part due to the low number of specimens with shear failure (only 32 cases, also 2 specimens with no transverse reinforcement were not included since the shear strength becomes zero). The good performance of the semi-empirical models is understandable due to the large database that was used for their calibration. However, these 2 semi-empirical models also show the largest differences between the number of specimens that are predicted with shear failure, indicating that such formulations might be highly dependent in the parameter selection, especially when more than one failure mode is expected.

The results indicate that the proposed model accurately predicts the shear strength of beam-column joints. Even, though the model presents good correlation, it is necessary to study the dependency to the main model parameters. Fig. 13 shows the same results presented in Fig. 12a, but in the horizontal axis different model parameters are deployed. The concrete compression strength (f'_c) is presented in Fig. 13a; the longitudinal reinforcement strength ($\rho_L f_{yL} + 0.3\rho_B f_{yB}$), similar to the contribution in Eq. (23) but for reinforcement yielding, in Fig. 13b; the transverse reinforcement strength ($\rho_t f_{yt}$) in Fig. 13c; and axial level ($N/f'_c A_g$) in Fig. 13d. As it can be seen in all plots of Fig. 13, there is

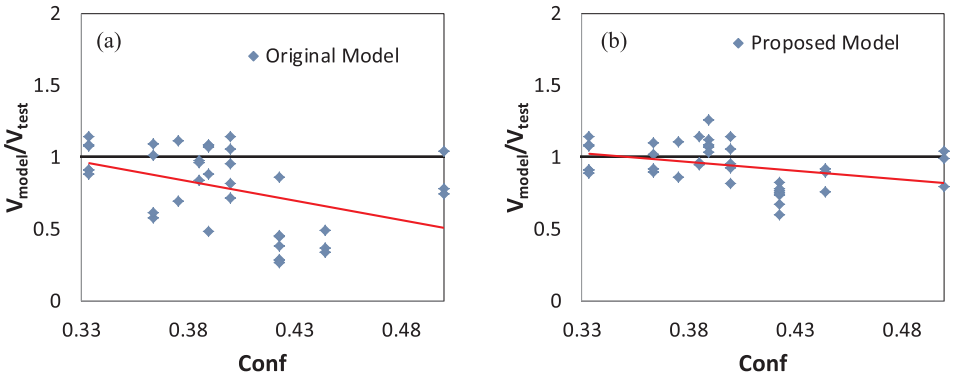

Fig. 11. V_{model}/V_{test} ratio respect to confinement level for interior joints – (a) original model, and (b) modified model.

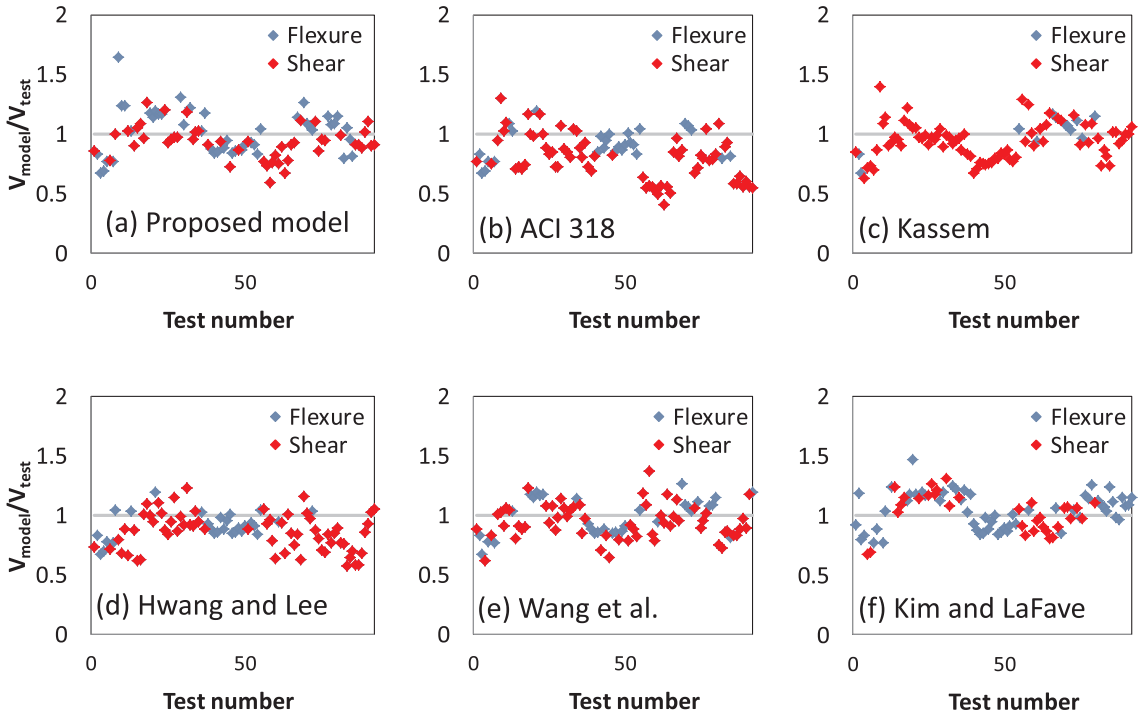

Fig. 12. Joint shear model to test strength ratio, V_{model}/V_{test}, – (a) proposed model, (b) ACI 318 [7]; (c) Kassem [8], (d) Hwang and Lee [5,6], (e) Wang et al. [10] and (f) Kim and LaFave [9].

modest dependency of the accuracy of the proposed model (V_{model}/V_{test}) to the parameters considered, indicating that their contribution is well captured by the model.

5. Conclusions

In the present work, a model is implemented with the objective of predicting the non-linear behavior of reinforced concrete beam-column joints subjected to axial and shear stresses, which is based on a simple formulation that considers an average strain and stress field of a reinforced concrete panel representing the joint. The model satisfies the equilibrium in the longitudinal direction.

A modification to the original model is developed, incorporating the confinement effect due to the presence of beams adjacent to the joint. For this, the transverse and longitudinal expansions are reduced (since the columns have a similar effect constraining the longitudinal strain), yielding new expressions for the crack angle, differentiating between exterior and interior joints, since the confinement effect of the beams for the interior joints is larger. Another modification incorporated is the constitutive law for concrete in tension, where the contribution of the transverse reinforcement is included.

After applying these modifications, the proposed model yields an average strength (V_{model}/V_{test}) of 0.97 and a standard deviation of 0.17, maintaining good estimates for both exterior and interior joints. This dispersion decreases to 0.14 when comparing only the specimens predicted to fail by joint shear. The incorporation of confinement for the estimation of the angle of the principal direction captures the dependence to the constraining of adjacent beams the joint, in particular with the interior joints, where the effect is more relevant.

The proposed model together with the work by Wang et al. [4] and the semi-empirical models (Kassem [8] and Kim and LaFave [9]) provide the best results, compared to others available in the literature, regarding their dispersion values and in terms of the average shear strength estimation. The semi-empirical models, however, present great differences in the number of specimens with shear failure. The proposed model can be used also to determine the entire shear load versus shear

Table 4
Strength estimate ratio for the proposed model and models from the literature.

Cases		Prop. model	ACI318	Hwang and Lee	Wang et al.	Kassem	Kim and LaFave
All	Average	0.97	0.83	0.87	0.96	0.95	1.03
	St. dev.	0.17	0.18	0.15	0.15	0.15	0.15
	C.O.V.	0.18	0.22	0.17	0.16	0.16	0.15
Joint shear	Average	0.93	0.79	0.86	0.94	0.94	1.04
	St. dev.	0.14	0.19	0.16	0.15	0.15	0.13
	C.O.V.	0.15	0.24	0.18	0.15	0.16	0.13
	N° cases (%)	47 (51%)	64 (70%)	64 (70%)	60 (65%)	80 (87%)	32 (36%)
Beam flexure	Average	1.02	0.93	0.91	1.00	1.02	1.03
	St. dev.	0.19	0.13	0.12	0.16	0.15	0.16
	C.O.V.	0.19	0.15	0.13	0.16	0.15	0.16
	N° cases (%)	45 (49%)	28 (30%)	27 (29%)	31 (35%)	11 (12%)	58 (64%)
Column flexo-comp.[a]	Average	–	–	0.94	0.94	0.94	0
	N° cases (%)	0 (0%)	0 (0%)	1 (1%)	1 (1%)	1 (1%)	0

[a] Only average is shown since there is 1 or 0 cases.

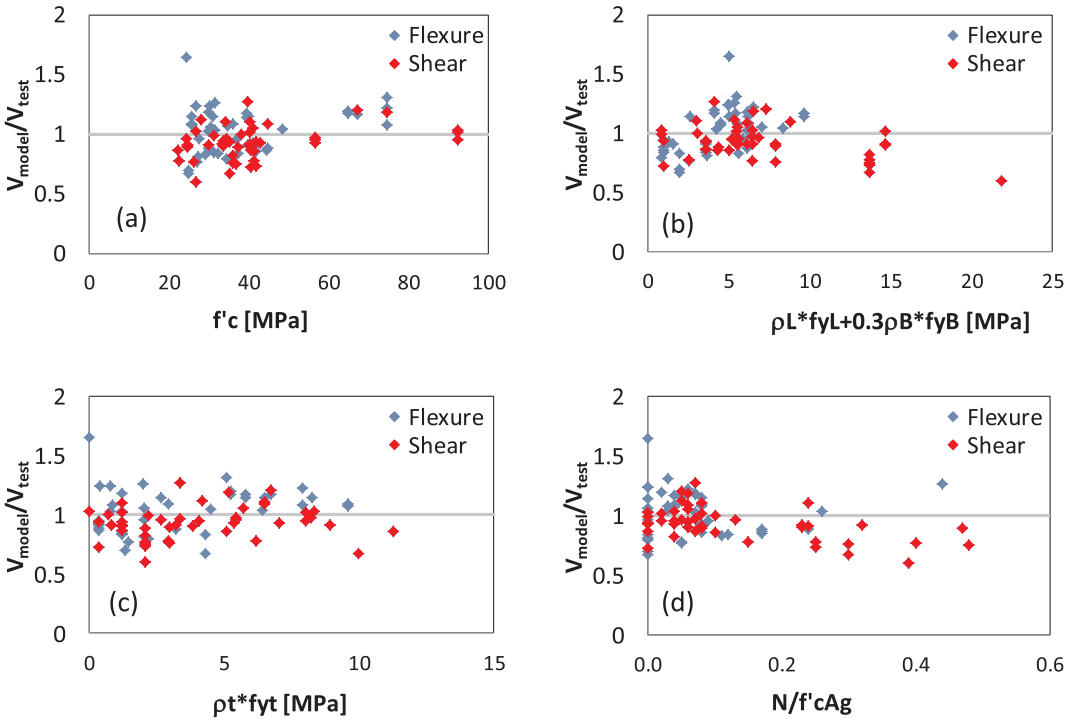

Fig. 13. Joint shear proposed model to test strength ratio, V_{model}/V_{test}, versus – (a) f'_c, (b) $\rho_L f_{yL} + 0.3\rho_B f_{yB}$; (c) $\rho_t f_{yt}$, and (d) $N/f'_c A_g$.

deformation of the joint.

References

[1] Hoffmann GW, Kunnath SK, Reinhorn AM, Mander JB. Gravity-load-designed reinforced concrete buildings: seismic evaluation of existing construction and detailing strategies for improved seismic resistance. Technical Report NCEER-92-0016. SUNY/Buffalo, NY: National Center for Earthquake Engineering Research; 1992.

[2] Youssef M, Ghobarah A. Modeling of RC beam-column joints and structural walls. J Earthq Eng 2001;5(1):93–111.

[3] Lowes LN, Altoontash A. Modeling reinforced concrete beam-column joints subjected to cyclic loading. J Strut Eng 2003;129(12):1686–97.

[4] Pan Z, Guner S, Vecchio FJ. Modeling of interior beam-column joints for nonlinear analysis of reinforced concrete frames. Eng Struct 2017;142:182–91.

[5] Hwang SJ, Lee HJ. Analytical model for predicting shear strengths of exterior reinforced concrete beam-column joints for seismic resistance. ACI Struct J 1999;96(5):846–57.

[6] Hwang SJ, Lee HJ. Analytical model for predicting shear strengths of interior reinforced concrete beam-column joints for seismic resistance. ACI Struct J 2000;97(1):35–44.

[7] ACI Committee 318. Building code requirements for structural concrete (ACI 318-14) and commentary (318R-14). Farmington Hills, Mich: American Concrete Institute; 2014.

[8] Kassem W. Strut-and-tie modelling for the analysis and design of RC beam-column joints. Mater Struct 2016;49:3459–76.

[9] Kim J, LaFave JM. A simplified approach to joint shear behavior prediction of RC beam-column connections. Earthq Spectra 2012;28(3):1071–96.

[10] Wang GL, Dai JG, Teng JG. Shear strength model for RC beam–column joints under seismic loading. Eng Struct 2012;40:350–60.

[11] Zhang L-XB, Hsu TTC. Behavior and analysis of 100 MPa concrete membrane elements. J Struct Eng 1998;124(1):24–34.

[12] Kupfer H, Gerstle KH. Behavior of concrete under biaxial stress. J Eng Mech Div, ASCE 1973;99(4):853–66.

[13] Kassem W, Elsheikh A. Estimation of shear strength of structural shear walls. J Struct Eng, ASCE 2010;136(10):1215–24.

[14] Massone LM, Ulloa MA. Shear response estimate for squat reinforced concrete walls via a single panel model. Earthq Struct 2014;7(5):647–65.

[15] Massone LM, Alvarez JE. Shear strength model for reinforced concrete corbels based on panel response. Earthq Struct 2016;11(4):723–40.

[16] Gupta A, Rangan BV. High-strength concrete HSC structural walls. ACI Struct J 1998;95(2):194–205.

[17] Massone LM. Strength prediction of squat structural walls via calibration of a shear-flexure interaction model. Eng Struct 2010;32(4):922–32.

[18] Fujii S, Morita S. Comparison between interior and exterior RC beam-column joint behavior. In: Jirsa JO, editor. Design of beam-column joints for seismic resistance, SP-123. Farmington Hills, Mich.: American Concrete Institute; 1991. p. 145–65.

[19] Ehsani MR, Wight JK. Exterior reinforced concrete beam-to-column connections subjected to earthquake-type loading. ACI J 1985;82(4):492–9.

[20] Durrani AJ, Wight JK. Behavior of interior beam-to-column connections under earthquake-type loading. ACI J 1985;82(3):343–9.

[21] Abrams DP. Scale relations for reinforced concrete beam-column joints. ACI Struct J 1987;84(6):502–12.

[22] Alameddine FF. Seismic design recommendation for high-strength concrete beam-to-column connections. PhD thesis, University of Arizona; 1990. 257p.

[23] Beckingsale CW. Post-elastic behaviour of reinforced concrete beam-column joints. Research Report No. 80-20. Department of Civil Engineering, University of Canterbury, Christchurch, New Zealand; 1980. 379p.

[24] Blakeley RWG, Megget LM, Priestley MJN. Seismic performance of two full-size reinforced concrete beam-column joint units. Bull New Zealand Nat Soc Earthq Eng 1975;8(1):38–69.

[25] Birss GR. The elastic behaviour of earthquake resistant reinforced concrete beam-column joints. Research Report No. 78-13. Department of Civil Engineering, University of Canterbury, Christchurch, New Zealand; 1978. 105p.

[26] Ehsani MR, Moussa AE, Vallenilla CR. Comparison of inelastic behavior of reinforced ordinary and high-strength concrete frames. ACI Struct J 1987;84(2):161–9.

[27] Fenwick RC, Irvine HM. Reinforced concrete beam-column joints for seismic loading. School of Engineering Report No. 142. Department of Civil Engineering, University of Auckland, Auckland, New Zealand; 1977. 50p.

[28] Kaku T, Asakusa H. Ductility estimation of exterior beam-column subassemblages in reinforced concrete frames. In: Jirsa JO, editor. Design of beam-column joints for seismic resistance, SP-123. Farmington Hills, Mich.: American Concrete Institute; 1991. p. 167–85.

[29] Kanada K, Kondon G, Fujii S, Morita S. Relation between beam bar anchorage and shear resistance at exterior beam-column joints. Trans Jpn Concr Inst 1984;6:433–40.

[30] Kitayama K, Otani S, Aoyama H. Development of design criteria for RC interior beam-column joints. Design of beam-column joints for seismic resistance, SP-123. Farmington Hills, Mich.: American Concrete Institute; 1991. p. 97–123.

[31] Lee DLN, Wight JK, Hanson RD. RC beam-column joints under large load reversals. J Struct Div, ASCE 1977;103(ST12):2337–50.

[32] Leon RT. Shear strength and hysteretic behavior of interior beam-column joints. ACI Struct J 1990;87(1):3–11.

[33] Megget LM. Cyclic behaviour of exterior reinforced concrete beam-column joints. Bull New Zealand Nat Soc Earthq Eng 1974;7(1):22–47.

[34] Meinheit DF, Jirsa JO. The shear strength of reinforced concrete beam-column joints. CESRL Report No. 77-1. Department of Civil Engineering, University of Texas at Austin; 1977. 271p.

[35] Otani S, Kitayama K, Aoyama H. Beam bar bond stress and behavior of reinforced concrete interior beam-column connections. Second U.S.-N.Z.-Japan Seminar, Tokyo; 1985.

[36] Park R, Gaerty L, Stevenson EC. Tests on an interior reinforced concrete beam-column joint. Bull New Zealand Nat Soc Earthq Eng 1981;14(2):81–92.

[37] Park R, Milburn JR. Comparison of recent New Zealand and United States seismic design provisions for reinforced concrete beam-column joints and tests results from four units designed according to the New Zealand code. Bull New Zealand Nat Soc Earthq Eng 1983;16(1):3–24.

[38] Paulay T, Scarpas A. Behavior of exterior beam-column joints. Bull New Zealand Nat Soc Earthq Eng 1981;14(3):131–44.

[39] Zerbe HE, Durrani AJ. Effect of slab on behavior of exterior beam-to-column connections. Report No. 30. Rice University, Houston, Tex.; 1985. 159p.